

ORIGINAL ARTICLE

# p53 protein aggregation promotes platinum resistance in ovarian cancer

Y Yang-Hartwich<sup>1</sup>, MG Soteras<sup>1</sup>, ZP Lin<sup>2</sup>, J Holmberg<sup>1</sup>, N Sumi<sup>1</sup>, V Craveiro<sup>1</sup>, M Liang<sup>1</sup>, E Romanoff<sup>1</sup>, J Bingham<sup>1</sup>, F Garofalo<sup>1</sup>, A Alvero<sup>1</sup> and G Mor<sup>1</sup>

High-grade serous ovarian carcinoma (HGSO), the most lethal gynecological cancer, often leads to chemoresistant diseases. The p53 protein is a key transcriptional factor regulating cellular homeostasis. A majority of HGSOs have inactive p53 because of genetic mutations. However, genetic mutation is not the only cause of p53 inactivation. The aggregation of p53 protein has been discovered in different types of cancers and may be responsible for impairing the normal transcriptional activation and pro-apoptotic functions of p53. We demonstrated that in a unique population of HGSO cancer cells with cancer stem cell properties, p53 protein aggregation is associated with p53 inactivation and platinum resistance. When these cancer stem cells differentiated into their chemosensitive progeny, they lost tumor-initiating capacity and p53 aggregates. In addition to the association of p53 aggregation and chemoresistance in HGSO cells, we further demonstrated that the overexpression of a p53-positive regulator, p14ARF, inhibited MDM2-mediated p53 degradation and led to the imbalance of p53 turnover that promoted the formation of p53 aggregates. With *in vitro* and *in vivo* models, we demonstrated that the inhibition of p14ARF could suppress p53 aggregation and sensitize cancer cells to platinum treatment. Moreover, by two-dimensional gel electrophoresis and mass spectrometry we discovered that the aggregated p53 may function uniquely by interacting with proteins that are critical for cancer cell survival and tumor progression. Our findings help us understand the poor chemoresponse of a subset of HGSO patients and suggest p53 aggregation as a new marker for chemoresistance. Our findings also suggest that inhibiting p53 aggregation can reactivate p53 pro-apoptotic function. Therefore, p53 aggregation is a potential therapeutic target for reversing chemoresistance. This is paramount for improving ovarian cancer patients' responses to chemotherapy, and thus increasing their survival rate.

*Oncogene* advance online publication, 29 September 2014; doi:10.1038/onc.2014.296

## INTRODUCTION

Ovarian cancer is the most lethal gynecological malignancy. Although most patients initially respond to chemotherapy, the majority succumb to recurrent chemoresistant tumors.<sup>1</sup> Efforts to overcome chemoresistance have been largely unsuccessful. The mortality rate remains high. High-grade serous ovarian carcinoma (HGSO) accounts for 67% of all ovarian cancers and is the most aggressive subtype. A main characteristic of HGSO is that 96% of the tumors bear p53 mutation.<sup>2</sup> p53 is a central transcriptional mediator. By binding to DNA, p53 controls the expression of hundreds of target genes in order to maintain homeostasis and genome integrity. In ~90% of ovarian cancers, one of the p53 alleles has a mutation that abrogates p53 transcriptional activity.<sup>3,4</sup> The other wild-type allele is usually also inactive or attenuated.<sup>5</sup> On the other hand, many tumors without p53 mutation still harbor a transcriptionally inactive form of p53,<sup>6–8</sup> suggesting that genetic mutation is not the only cause of p53 inactivation. Therefore, the presence of wild-type (wt) p53 does not necessarily indicate good prognosis and chemoresponse. In the case of HGSO, patients with wt p53 have even poorer survival rates and are more chemoresistant than those with mutant p53.<sup>9</sup> Therefore, additional mechanisms of p53 inactivation beyond genetic mutations need to be further studied.

Recently, it has been shown that in different types of cancer cell lines and tumors, both mutant and wt p53 protein can aggregate into amyloid fibrils.<sup>10–13</sup> Protein aggregation is a pathogenic feature of a growing number of diseases, such as Alzheimer's and Parkinson's disease.<sup>14</sup> *In vitro* studies suggest that p53 is an amyloid-forming protein. Amyloid-forming proteins are an unusual subset of proteins that are able to aggregate. Although the amino-acid sequences of these proteins are diverse, they all adopt a similar, highly organized structure upon aggregation known as the cross- $\beta$  spine that consists of an ordered arrangement of  $\beta$ -sheets. The transactivation, DNA-binding and tetramerization domains of p53 protein can all misfold and form amyloid fibrillar aggregates.<sup>15–19</sup> Protein aggregation can perturb essential cellular functions and cause various human disorders.<sup>20</sup> Considering the crucial role of p53 in maintaining cellular homeostasis, the aggregation of p53 may affect its normal functions and act as a key factor in the initiation and progression of cancer.<sup>21,22</sup>

Cancer stem cells (CSCs) are a subpopulation of chemoresistant tumor cells that can give rise to heterogeneous tumors through self-renewal and multilineage differentiation. CSCs were shown to exist in hematologic and solid cancers<sup>23–25</sup> including ovarian cancer.<sup>26–28</sup> The CSC model explains much of ovarian cancer's etiology, such as tumor dormancy, minimal residual disease, drug

<sup>1</sup>Department of Obstetrics and Gynecology, Yale University School of Medicine, New Haven, CT, USA and <sup>2</sup>Department of Pharmacology, Yale University School of Medicine, New Haven, CT, USA. Correspondence: Professor G Mor, Division of Reproductive Sciences, Department of Obstetrics, Gynecology and Reproductive Sciences, Yale University School of Medicine, 333 Cedar Street, LSOG 305A, New Haven, CT 06520, USA.

E-mail: gil.mor@yale.edu

Received 19 March 2014; revised 25 June 2014; accepted 31 July 2014

resistance and disease relapse. Ovarian cancer stem cells (OCSCs) have been identified with different markers. We identified a population of CD44+/MyD88+ OCSCs that can initiate tumors in immunocompromised mice and differentiate into multiple cell types including CD44-/MyD88- ovarian cancer cells (OCCs).<sup>29–31</sup> More important, CD44+/MyD88+ OCSCs are *in vivo* and *in vitro* resistant to currently available chemotherapeutic agents, including taxane- and platinum-based agents.<sup>29,32</sup> Among the CD44+/MyD88+ OCSCs isolated from > 100 ovarian cancer samples, we have identified two cell lines with wt p53. They are highly resistant to platinum-based agents and have been used as a model of OCSCs with p53 aggregates in our study. We hypothesize that the aggregation of p53 can inhibit its pro-apoptotic functions and promote chemoresistance in OCSCs.

The objectives of this study are twofold. First, we determine whether p53 aggregation is associated with the loss of p53 pro-apoptotic functions and chemoresistance. Second, we explore the potential molecular mechanisms causing p53 aggregation. It is hypothesized that the formation of protein aggregates depends on protein concentration, complex interactions with other proteins and specific cellular environment.<sup>33</sup> However, the cause of p53 aggregation in tumors is still unclear. We propose that

inefficient protein degradation leads to the accumulation of misfolded p53 proteins and induces aggregation.

Using the OCSC model, we have uncovered that MDM2 is inhibited by an antagonist p14ARF (ARF), and the lack of MDM2-mediated degradation can cause p53 to accumulate and form aggregates. ARF is a tumor-suppressor protein that binds to MDM2 and inhibits the E3 ligase activity of MDM2, leading to p53 protein stabilization. ARF also promotes MDM2 degradation and sequesters MDM2 into the nucleolus.<sup>34–37</sup> It is well known that MDM2/MDM4 overexpression causes p53 inhibition.<sup>38</sup> The amplification of MDM2/MDM4 is frequently observed in tumors.<sup>39</sup> Our *in vitro* and *in vivo* data reveal a paradoxical mechanism by which the inhibition of MDM2 by ARF can result in p53 inactivation and chemoresistance by causing the imbalance of p53 turnover, and p53 protein aggregation.

## RESULTS

CD44+ OCSCs, but not their CD44- progeny OCCs, possess tumorigenicity and chemoresistance

Utilizing the previously reported method,<sup>29,30</sup> we isolated a population of CD44+/Myd88+ OCSCs from HGSOC tumors. CD44

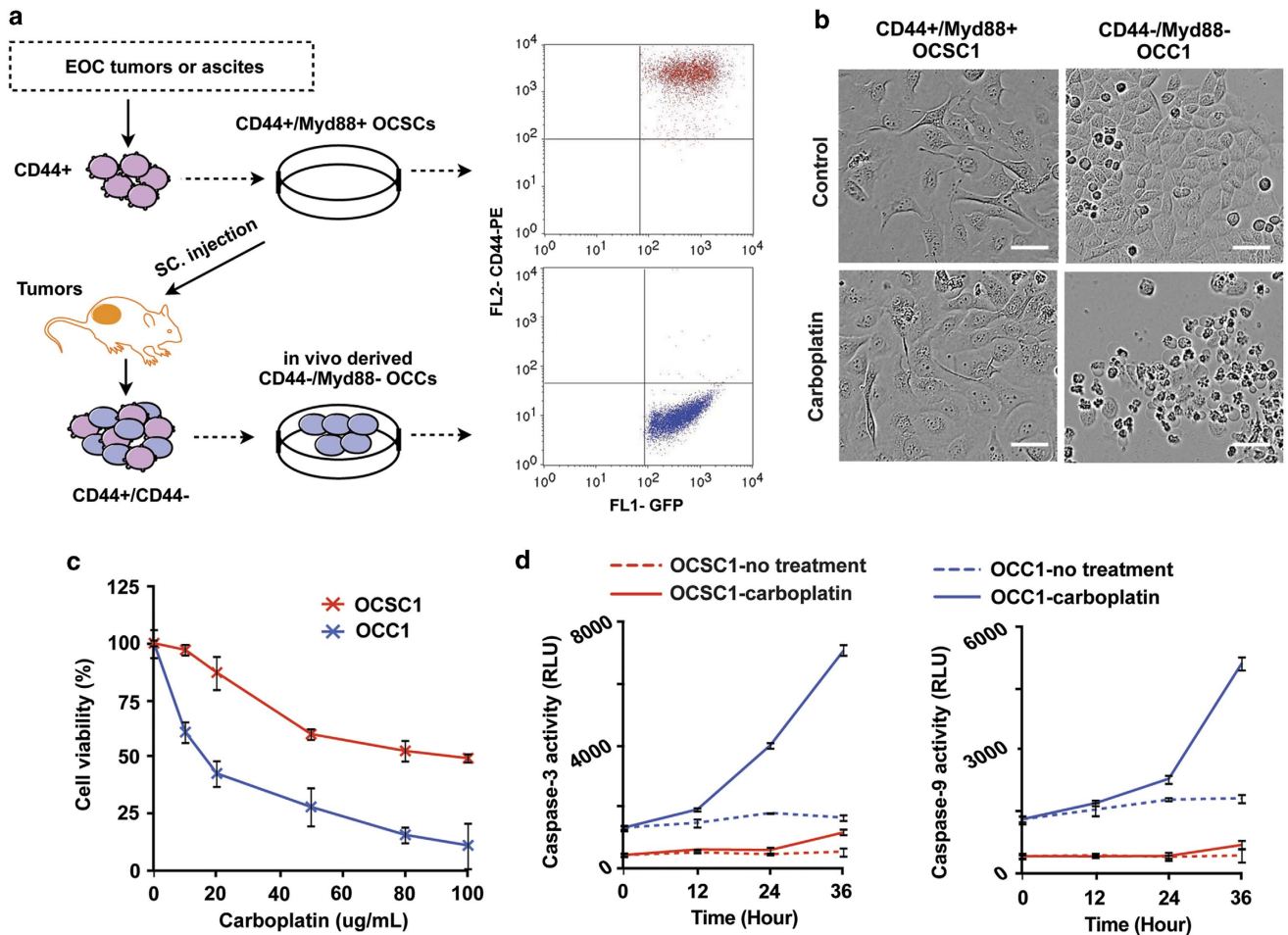


**Figure 1.** CD44+ OCSC1s but not their progeny CD44- OCC1s possess cancer stem cell properties. **(a)** Schematic representation of the isolation of OCSCs and OCCs. CD44+ OCSCs are isolated from HGSOC tumors or ascites by flow sorting and cultured. They were infected by lentivirus expressing GFP and then subcutaneously injected to immunocompromised mice. From the formed tumors, GFP+/CD44- OCCs are isolated and cultured. Fluorescence-activated cell sorting (FACS) analysis (dot plot) indicates that GFP+/CD44+ OCSCs can *in vivo* differentiate into GFP+/CD44- OCCs. **(b)** Morphology changes of OCSC1s and OCC1s in carboplatin treatment. **(c)** Dose-dependent viability of OCSC1s (red) and OCC1s (blue) treated with carboplatin. **(d)** Caspase-3 (left) and caspase-9 (right) activities of nontreated (dotted) and carboplatin-treated (solid) OCSC1s (red) and OCC1s (blue).

+Myd88+ OCSCs possess cancer stem cell properties including tumor-initiating capability (Supplementary Figures 1a–c). To demonstrate that these OCSCs have tumor formation and differentiation capacity, we labeled them with green fluorescent protein (GFP)-expressing lentivirus and subcutaneously injected them into immunocompromised mice (Figure 1a). CD44+/GFP+ OCSCs formed heterogeneous tumors consisting of both CD44+/GFP+ and CD44–/GFP+ cells. The CD44–/GFP+ cells isolated from these tumors lost cancer stem cell properties and cannot form tumors in mice (Figure 1a and Supplementary Figures 1a–d and 2a). We named them CD44– OCCs.

In this study, we selected two OCSC clones with wild-type p53 that were isolated from two individual patients. The OCC lines were derived from both OCSC clones. These two sets of cell lines were named OCSC1/OCC1 and OCSC2/OCC2 (Supplementary Figures 1 and 2a, respectively). The p53 mutation analysis was performed on these cells by sequencing full-length p53 complementary DNA (cDNA) and exons 5–8 of *TP53* gene (encoding the DNA-binding domain of p53 protein that is frequently mutated). We did not detect p53 mutations in OCSC1, OCC1, OCSC2 or OCC2 (Supplementary Tables 1 and 2). We did not detect the overexpression of dominant-negative p53 isoforms or  $\Delta$ N-p63 (data not shown).

OCSCs are chemoresistant. When they differentiated into OCCs, they become chemosensitive. For example, when treated with carboplatin (50  $\mu$ g/ml for 48 h), OCSC1s maintained their normal morphology. The same treatment induced significant cell death in OCC1s (Figures 1b and c). We detected the induction of caspase-3 and -9 activities after carboplatin treatment in OCC1 and OCC2, but not in OCSC1 and OCSC2 (Figure 1d and Supplementary Figures 2b and c). Together, our data demonstrate that OCSCs, but not their progeny OCCs, possess tumor-initiating properties and resistance to platinum-based treatment.

The p53 protein aggregation is associated with p53 inactivation in OCSCs

By immunofluorescent staining, we detected that OCSCs expressed high levels of p53 (Figure 2a and Supplementary Figure 3d). At the same time, we observed the presence of aggregates in OCSCs. We performed immunofluorescent staining with thioflavin T, a fluorescent dye that labels amyloid aggregates<sup>40</sup> and anti-amyloid fibril antibody (OC, an antibody recognizing generic epitopes common to amyloid fibrils and oligomers<sup>41</sup>). OCSCs and OCCs were co-stained for aggregates and p53 (Figures 2a and b and Supplementary Figures 3a and b). OCSCs showed widespread protein aggregation that colocalized with p53 staining in both the control and carboplatin-treated groups. The positive staining localized in both nuclei and cytoplasm. However, it mainly concentrated in the nuclei (Supplementary Figure 4). OCCs were negative for protein aggregation, even when p53 protein accumulated following carboplatin treatment. When we knocked down the expression of p53 in OCSC1 with small hairpin RNA (shRNA), the levels of aggregates detected by staining were significantly decreased (Supplementary Figure 5). Our observation differed from the previous report that showed cytoplasmic distribution of p53 aggregates.<sup>11</sup> In the nuclei of OCSCs, the levels of aggregates are much higher than in their cytoplasm that was in a similar pattern as p53 levels. Our observation indicates that in OCSCs most of the p53 proteins were translocated into the nucleus and form aggregates in the nucleus, and this is different from the aggregates from mutant p53 in the previous report.<sup>11</sup> The nuclear environment may have a role in regulating the formation of these aggregates.

Western blots from non-denaturing gels (native polyacrylamide gel electrophoresis) confirmed the presence of high-molecular-weight p53 aggregates in OCSC1, but not in OCC1 (Figure 2c).

Anti-amyloid fibril dot blots showed that OCSC1 and OCSC2 were positive for protein aggregation, whereas OCC1 and OCC2 were negative (Figure 2d and Supplementary Figure 3c). We hypothesized that the aggregation of p53 protein led to p53 inactivation in OCSCs that might contribute to the resistance to chemotherapies.

The inactivation of p53 is associated with the attenuated ability of p53 to bind to DNA and activate downstream target gene expression. To test the effect of aggregation on p53 activity, we tested whether the transactivation of wt p53 was inhibited in OCSC1 and OCSC2. The p53 chromatin immunoprecipitation data indicated that the binding of p53 to the promoter of *MDM2*, *P21* and *Puma* was inhibited in OCSC1s when compared with OCC1s. Carboplatin treatment slightly increased p53 DNA binding in OCSC1, whereas in OCC1s carboplatin significantly increased p53 DNA binding (Figure 2e). Quantitative reverse transcriptase-PCR of p53 target genes, including *MDM2*, *P21*, *Puma*, *Bax* and *Fas*, showed consistent result. In OCC1s when p53 DNA binding was increased by carboplatin treatment, the target gene transcription was consequently upregulated (Figure 2f). On the contrary, in OCSC1s the inhibited p53-DNA binding led to the inhibited response of p53 target gene transcription. Carboplatin treatment failed to upregulate p53 target gene mRNA (Figure 2f). Similar results were observed in OCSC2s and OCC2s (Supplementary Figures 3b and d). Our data indicate that the transactivation of wt p53 was inhibited in OCSCs and restored when they differentiated into OCCs.

In order to determine whether the *in vitro* observations are also present in tumor samples, we performed a study that included 32 ovarian tumor biopsies (Supplementary Table 3). We detected the presence of protein aggregates in almost half of the samples. More important, we found a significant correlation between p53 overexpression and protein aggregation (Figure 2g and Supplementary Figure 6). Out of 18 patients with high p53 levels, 13 patients had protein aggregates. Out of 14 patients with low p53 levels, 13 patients showed low levels of aggregation. Based on the amyloid-forming nature of p53 protein and our *in vitro* data, we conclude that the overexpressed p53 protein is involved in the aggregates, associated with the inhibition of p53 transcriptional activity in OCSCs.

ARF overexpression inhibits p53 degradation in OCSCs

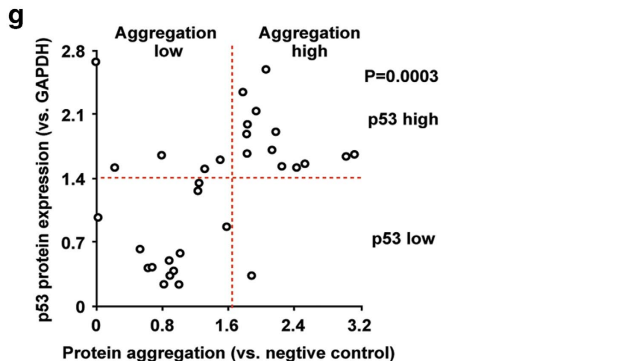
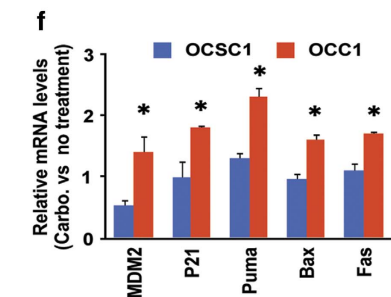
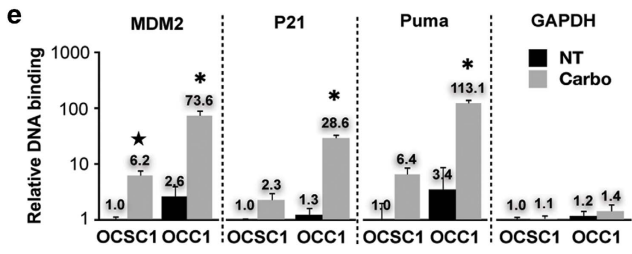
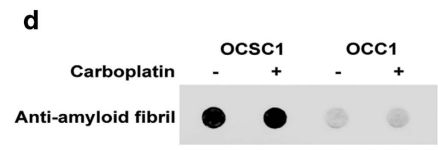
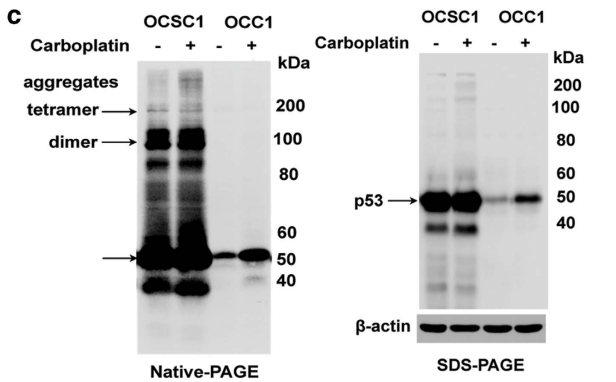
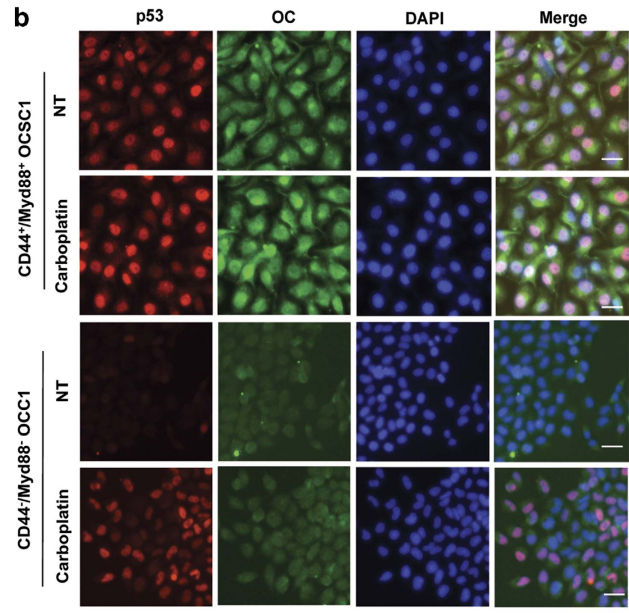
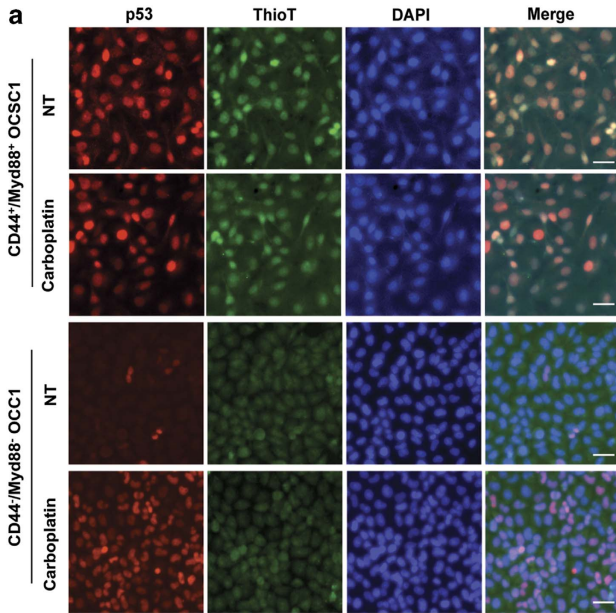
Using immunofluorescent staining and western blot, we detected high levels of p53 protein in OCSC1s and OCSC2s regardless of carboplatin treatment. Conversely, OCC1s and OCC2s expressed low basal levels of p53 protein. However, following carboplatin treatment, OCC1s and OCC2s showed significant increase of p53 protein level and nuclear translocation (Figures 2a and 3a and Supplementary Figure 3a). OCC1 also showed a significant upregulation of *MDM2* in response to carboplatin. Conversely, the *MDM2* expression did not change in OCSC1s following carboplatin treatment (Figure 3a).

*MDM2* and *MDM4* are the major regulators of p53 protein degradation. OCCs expressed higher levels of *MDM2* and *MDM4* than OCSCs (Figure 3a and Supplementary Figure 7). However, we did not observe differences between OCSC1s and OCC1s in *MDM2* mRNA level (Figure 3b). When OCSC1s were treated by a proteasome inhibitor, MG132, the level of *MDM2* protein in OCSCs was significantly upregulated, suggesting that *MDM2* is rapidly degraded in OCSC1s (Figure 3c). Interestingly, when we overexpressed *MDM2*, the degradation of p53 was induced in OCC1s, but not in OCSC1s (Figure 3d). These findings indicate the presence of factor(s) that can promote *MDM2* degradation and inhibit *MDM2*-mediated p53 degradation, leading to p53 accumulation in OCSCs.

Tumor suppressor ARF binds to *MDM2*, inhibits the E3 ligase activity of *MDM2*, promotes *MDM2* degradation and sequesters

MDM2 into the nucleolus. By western blot we detected the overexpression of ARF in OCSC1s (Figure 3a). To determine whether there is a correlation between the overexpression of ARF

and p53, we knocked down ARF mRNA and protein expression in OCSC1s using two lentiviral shRNAs: shARF1 and shARF2. Inhibition of ARF in OCSC1 led to MDM2 stabilization and the



degradation of p53 (Figure 3e). These data suggest that high levels of ARF in OCSCs inhibit MDM2 function and lead to p53 accumulation.

ARF is activated by oncogenic insults. As the tumor progresses, ARF is often inactivated by deletion, mutation or epigenetic silencing, such as promoter DNA methylation.<sup>42</sup> We hypothesize that when OCSC1s differentiate into OCC1s, epigenetic silencing caused the decrease of ARF expression that may indirectly reverse p53 aggregation. We next examined ARF promoter status by methylation-specific PCR. ARF promoter is unmethylated in OCSC1s. In OCC1s, it is partially methylated that is sufficient to suppress ARF expression (Figure 3f). We evaluated the ARF status of 17 cancer cell lines derived from ovarian cancer biopsies. Based on their phenotypes including CD44 expression levels (Figure 3g), growth rate, morphology and chemoresistance (data not shown), the cell lines were categorized as either OCSC type or OCC type. The methylation-specific PCR results showed that in 10 OCSC-type cell lines, ARF promoter was unmethylated, and ARF mRNA levels were significantly higher, whereas 7 OCC-type cell lines showed different levels of methylation and low levels of ARF mRNA (Figures 3g and h).

ARF silencing reverses p53 aggregation and sensitizes OCSCs to carboplatin treatment

Misfolded polypeptides and damaged mature proteins are degraded in cells via ubiquitination or autophagy.<sup>43,44</sup> Inefficient proteasome degradation leads to protein aggregation affecting normal cellular functions. We postulated that the overexpressed ARF inhibited MDM2-mediated p53 degradation, resulting in the accumulation of misfolded p53. The p53 protein formed aggregation that inhibited normal p53 functions in OCSCs (model shown in Figure 4a, left). We therefore examined whether inhibiting ARF can decrease p53 aggregation. Indeed, ARF knockdown diminished protein aggregation, and had the similar effect as knocking down p53 with shRNA (shp53, Figure 4b and Supplementary Figure 6). Moreover, inhibiting ARF restores p53 function and sensitizes OCSC1s to carboplatin treatment (Figure 4c). Our data suggest that when OCSCs differentiate into OCCs, ARF gene silencing by promoter methylation indirectly impedes p53 aggregation, restoring the function of p53 (model shown in Figure 4a, right).

Using a co-culture model, we tested whether it is possible to sensitize heterogeneous tumors to carboplatin by inhibiting p53 aggregation with ARF knockdown. GFP-labeled OCSC1s and mCherry-labeled OCC1s were mixed and cultured together, mimicking heterogeneous tumors. Upon 48 h of carboplatin treatment followed by 48 h of recovery, the only cells that survived were GFP-OCSC1s. When ARF was inhibited in OCSCs by shARF2, we were able to eliminate all the cancer cells with carboplatin (Figure 4d).

We then tested whether we could reverse chemoresistance using an *in vivo* xenograft model. The mCherry-labeled control pLKO-OCSC1s or shARF2-OCSC1s were injected intraperitoneally into immunocompromised mice. shARF2 does not significantly affect the tumor-forming ability of OCSC1s (Supplementary Figure 8). During cisplatin treatment, tumors in the control group showed significant progression, whereas no significant tumor growth was observed in the shARF group (Figures 5a and b). Non-denaturing gel and western blot analysis showed that the high-molecular-weight p53 aggregates were downregulated by shARF2 (Figure 5c). In the cisplatin-treated groups, shARF tumors showed significantly higher levels of active caspase-3 and -9 when compared with the control pLKO tumors (Figures 5d and e). Morphologically, cisplatin induced extensive cell death in shARF tumors but did not affect control pLKO tumors (Figure 5f). Collectively, our data suggest that cisplatin resistance of OCSC-formed tumors is associated with high levels of p53 aggregates. ARF knockdown can inhibit p53 aggregation, restore p53 function and sensitize tumors to cisplatin treatment.

Aggregated p53 gain of function

Next, we determined whether the aggregated p53 (AGp53) gained the ability to interact with other proteins and potentially contributed to tumor progression. We analyzed p53 protein complex that was immunoprecipitated from carboplatin-treated OCSC1s and OCC1s using two-dimensional gel electrophoresis (Supplementary Figure 9). Our analysis indicated a compelling difference in the profile of p53-binding proteins in OCSC1 with AGp53 and OCC1 with normal wt p53. Using mass spectrometry, we identified a list of proteins that were significantly enriched in the p53 protein complex of OCSC1 (Table 1). These proteins are involved in multiple essential cellular functions, including cytoskeletal functions, RNA processing, transcription and translation, indicating that p53 aggregation may facilitate tumor progression through affecting these functions.

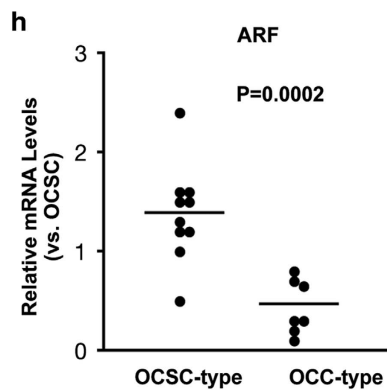
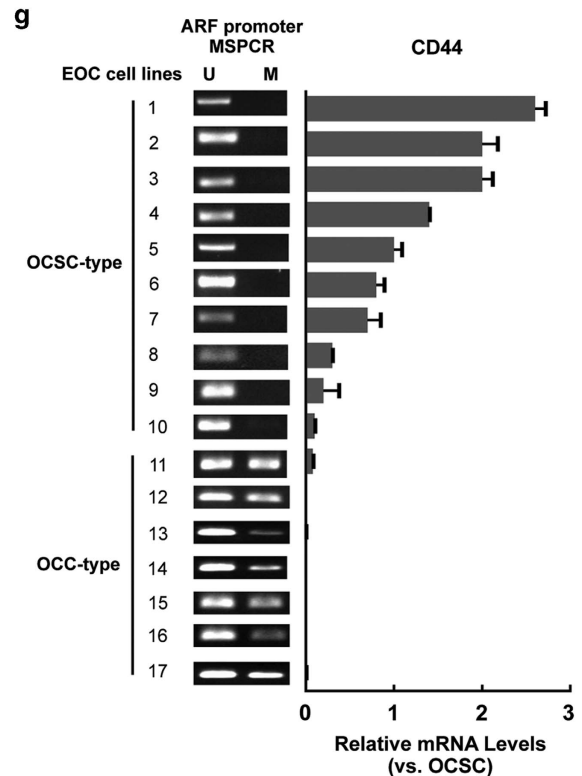
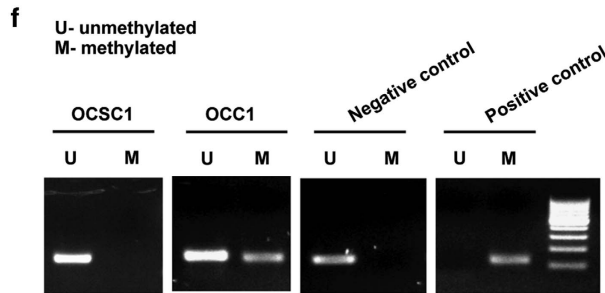
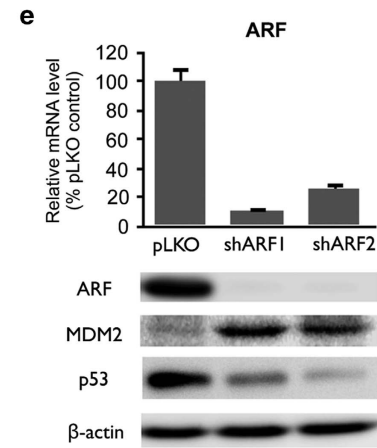
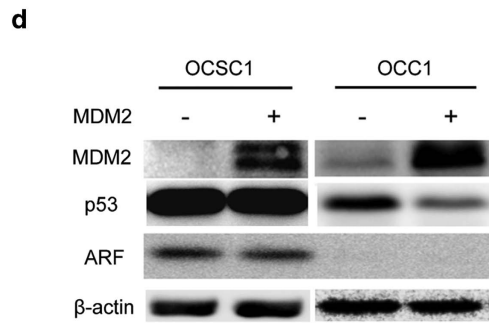
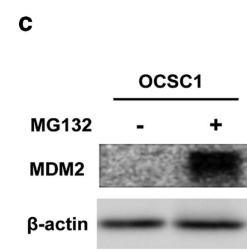
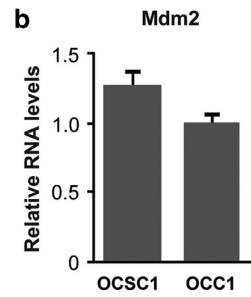
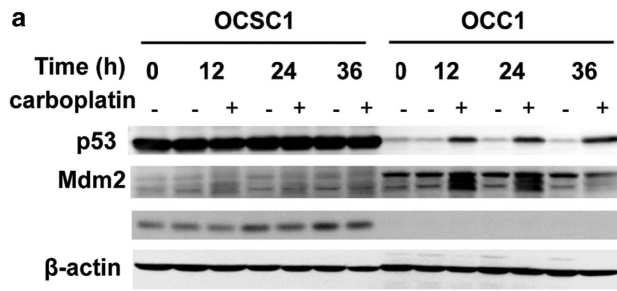
## DISCUSSION

We demonstrate that in a population of CD44+ OCSCs, defective MDM2-mediated degradation causes p53 protein aggregation. The aggregation sequesters native p53 protein into an inactive conformation lacking pro-apoptotic functions that correlates with resistance to carboplatin treatment. Our data reveal a more complex scenario of the p53 status and emphasize that in addition to genetic mutations, the imbalanced proteostasis can also inactivate p53. Notably, p53 aggregation is cell-type specific and associated with cancer cells with cancer stem cell properties. Furthermore, we demonstrate that overexpression of ARF may be responsible for p53 aggregation. The inhibition of ARF can restore p53 degradation and is sufficient to suppress p53 aggregation and reverse chemoresistance.

**Figure 2.** The p53 protein aggregation is associated with p53 inactivation in OCSC1s. **(a)** Co-immunofluorescence staining of p53 (red) and amyloid fibrils by Thioflavin T (ThioT, green). Nuclei were stained with 4',6-diamidino-2-phenylindole (DAPI, blue). Merged images show the overlap of p53 and ThioT staining (yellow or orange). Scale bars are 36  $\mu$ m. **(b)** Co-immunofluorescence staining of p53 (red) and amyloid fibrils (anti-amyloid fibril antibody, OC, green). Merged images show the overlap of p53 and OC staining (yellow or orange). Scale bars are 36  $\mu$ m. **(c)** P53 western blot of non-denaturing gel (native polyacrylamide gel electrophoresis (PAGE)) and denaturing gel (SDS-PAGE). In the presence of aggregates, p53 protein shifted to higher molecular weight. **(d)** Dot blot of amyloid fibrils in carboplatin treated (+) and nontreated (-) OCSC1 and OCC1. **(e)** Chromatin immunoprecipitation (CHIP)-quantitative PCR (qPCR) analysis of p53 DNA binding. Cells were nontreated (NT, black) or carboplatin-treated (Carbo, gray). Primers for qPCR target the p53-binding sites in MDM2, p21 and puma promoter. Data were normalized to nontreated OCSC1s. GAPDH was included as PCR negative control. IP IgG was used as IP negative control. \* $P < 0.05$  vs NT OCSC1. \* $P < 0.05$  vs NT OCC1. **(f)** Reverse transcriptase (RT)-qPCR of p53 target genes. OCSC1s (blue) and OCC1s (red) were treated by carboplatin. Data were normalized to the respective nontreated OCSC1s or OCC1s. \* $P < 0.05$  vs nontreated control. **(g)** Correlation analysis of p53 expression and protein aggregation in tumor biopsies ( $n = 32$ ). p53 western blot and protein aggregation dot blot were quantified. The statistical significance of the correlation between p53 overexpression and protein aggregation is tested by Fisher's exact test ( $P$ -value is indicated in the graph). The above data represent the means  $\pm$  s.d. of three technical replicates.

ARF is a key mediator of p53–MDM2 interaction. In addition to showing the correlation of ARF overexpression and p53 aggregation, we were able to inhibit aggregation and reactivate p53 by knocking down ARF. To our knowledge, this is the first

demonstration of a mechanism causing endogenous p53 aggregation in cancer cells. When OCSCs differentiated into OCCs, ARF was silenced via ARF promoter methylation that potentially restored p53 degradation and inhibited aggregation,



consequently reactivating the pro-apoptotic function of p53. We have described a unique epigenetically regulated process of reversing endogenous protein aggregation during cell-type transition.

The formation of high-molecular-mass species and self-aggregation of p53 was first described in the early 1990s.<sup>45</sup> Later, the prion-like characteristics of p53 protein were demonstrated *in vitro*.<sup>15–18</sup> More recent studies have shown the presence of p53 aggregates in cancer cell lines and tumor samples, including breast cancer, colorectal cancer, skin cancer and neuroblastoma.<sup>11,12,22</sup> However, p53 aggregation had not been studied in ovarian cancer. Our data suggest that the presence of protein aggregates is not rare in ovarian tumors. Protein aggregation is often associated with p53 overexpression in ovarian tumors. The molecular evidences we provide raise the possibility that p53 protein aggregation is responsible for chemoresistance in a subset of ovarian cancers.

In the present study we utilized two chemoresistant ovarian cancer cell lines with wt p53. We provided evidence supporting that the overexpressed p53 in OCSCs is indeed wild type, even though it lacks pro-apoptotic function. First, no mutations were detected by DNA or cDNA sequencing. Second, the dominant-negative isoforms of p53 were not detected. Third, once OCSCs differentiated into OCCs, protein aggregation diminished and p53 pro-apoptotic functions were restored, resulting in OCSCs responsive to carboplatin.

The model with wt p53 aggregation described in this study is important as it allows us to study the effects of aggregation and genetic mutation separately. We can study how protein aggregation attenuates p53 activity without the involvement of mutant p53 dominant-negative effects and gain of function. Moreover, our model may explain why HGSOC patients with wt p53 showed poorer survival rates and were more chemoresistant than those with mutant p53.<sup>9</sup>

The formation of aggregates is not limited to wt p53. The majority of ovarian tumors have one mutant p53 allele. Many ovarian tumors have the type of mutation with aggregation-driven dominant-negative effect.<sup>3,11</sup> These mutations can inactivate wt p53 allele by aggregating with wt p53 protein. A number of these mutations also exert gain of functions, such as binding to new target DNA or proteins. Thus, the behaviors of mutant p53 aggregates are more complex and difficult to study. Our model provides the basis for the characterization on how mutant p53 aggregates affect p53 function and chemoresistance. The formation of aggregates in cancer cells is neither limited to p53 protein. Our staining results showed that the anti-amyloid fibril antibody staining did not completely overlap with p53 staining in the cytoplasm, indicating that there are other proteins involved into aggregation in the cytoplasm. When p53 was very effectively knocked down by shRNA, we detected significant decreased levels of aggregates by anti-amyloid fibril dot blot (Figure 4b). However, low levels of aggregates were still present. The staining result showed that

knockdown of p53 diminished the nuclear staining of anti-amyloid fibril antibody (Supplementary Figure 7), but low levels of aggregates were still present in the cytoplasm. These results also indicate the existence of aggregates formed by other proteins in the cytoplasm.

The association of p53 aggregation and tumor progression was recently reported.<sup>11,46,47</sup> For instance, by coaggregation, p53 aggregation can inactivate p63 and p73, leading to an increase in oncogenic potential in cells.<sup>11</sup> The mechanisms of p53 aggregation promoting tumor progression still need to be further elucidated. In our system, the protein-binding profile of AGp53 reveals potential related pathways (Table 1). Cytoskeleton proteins are among AGp53-associated proteins. This is consistent with a previous report showing that protein aggregates interact with cytoskeletal architecture,<sup>20</sup> thus interfering with intracellular transport and cell division.

We found a group of translation initiation factors (EIF2 and EIF3 subunits) interacting with AGp53, possibly altering global protein synthesis of OCSCs. Notably, AGp53 shows increased binding with topoisomerase-1 (TOP1) that may cause increased DNA repair and genetic instability in OCSCs, as p53 enhances TOP1 catalytic activities of genetic recombination.<sup>48</sup> In addition, AGp53 interaction with heat shock protein 90 (HSP90) strengthens our theory that protein aggregation drives wt p53 into the mutant phenotypic form, as only the mutant p53 recruits HSP90 to inhibit ubiquitination turnover, resulting in p53 stabilization.<sup>49</sup> Studying the protumor cellular functions of AGp53 will identify novel therapeutic targets.

Overexpression of p53 in tumors is generally interpreted as a sign of *TP53* gene mutation and represents a hallmark of cancer. However, the independent prognostic value of aberrant p53 status (expression level and mutation) remains controversial. The aggregation of p53 is a new parameter that helps us assess p53 status. Using fibril-specific, conformation-dependent antibodies recognizing generic epitopes, protein aggregates can be identified within tumor samples. By co-staining with p53 it is possible to detect p53 aggregates in tumor biopsies as a marker for platinum resistance. As many of the HGSOC tumors retain at least one wt p53 allele, reactivation of wt p53 through suppressing aggregation is a promising therapeutic strategy.

Our study demonstrates a cell-specific regulation of p53 protein stabilization associated with protein aggregation that confers chemoresistance. The correlation between p53 aggregation and platinum resistance is relevant to understand the poor prognosis of patients with HGSOC. Use of p53 aggregation as a marker would allow the stratification of these patients and personalized therapy. Furthermore, aggregation inhibitors can be potential chemosensitizers in combination with platinum-based therapies to eliminate resistant cancer stem cells and prevent recurrence (Figure 6). In order to fully understand the role of p53 aggregation in ovarian cancer and its value as a prognostic marker or a therapeutic target, cancer cell lines and tumor samples with a

**Figure 3.** The overexpression of ARF causes p53 accumulation in OCSCs. (a) Western blots of p53 and MDM2 in OCSC1s and OCC1s treated by carboplatin. (b) Reverse transcriptase–quantitative PCR (RT–qPCR) analysis of MDM2 expression in OCSC1s and OCC1s. (c) Western blots of MDM2 in OCSC1s treated by 5  $\mu$ M MG132 for 24 h. (d) Western blots of MDM2 and p53 in OCSC1s and OCC1s transfected by pcDNA-MDM2 (+) or control vector (–) plasmid. (e) RT–qPCR analysis (upper) of ARF mRNA and western blots (lower) of ARF, MDM2 and p53 in control pLKO-OCSCs (infected by pLKO vector), shARF1-OCSCs and shARF2-OCSCs (infected by lentiviral shRNAs targeting ARF). (f) Gel electrophoresis of methylation-specific PCR (MS-PCR). DNA products were amplified from bisulfite-converted DNA of OCSCs and OCCs. The unmethylated (U) and methylated (M) ARF promoters were detected by specific primers. Normal ovarian surface epithelial (OSE) cell DNA is used as a negative control. CpG Methyltransferase (M.SssI)-treated OSE DNA is a positive control for ARF promoter methylation. (g) MSPCR analysis of ARF promoter (M, methylated; U, unmethylated) and RT–qPCR analysis of CD44 expression in cancer cell lines derived from 17 advanced ovarian tumor biopsies. They were classified as OCSC type ( $n = 10$ ) or OCC type ( $n = 7$ ) based on their phenotypes. Data are normalized to OCSC1s. The above data represent the means  $\pm$  s.d. of three technical replicates. (h) RT–qPCR analysis of ARF expression in OCSC-type and OCC-type cancer cell lines. Data are normalized to OCSC1s. Each dot represents one cell line. Bars represent the mean of each group. The two groups are significantly different ( $P$ -value is indicated in the graph).

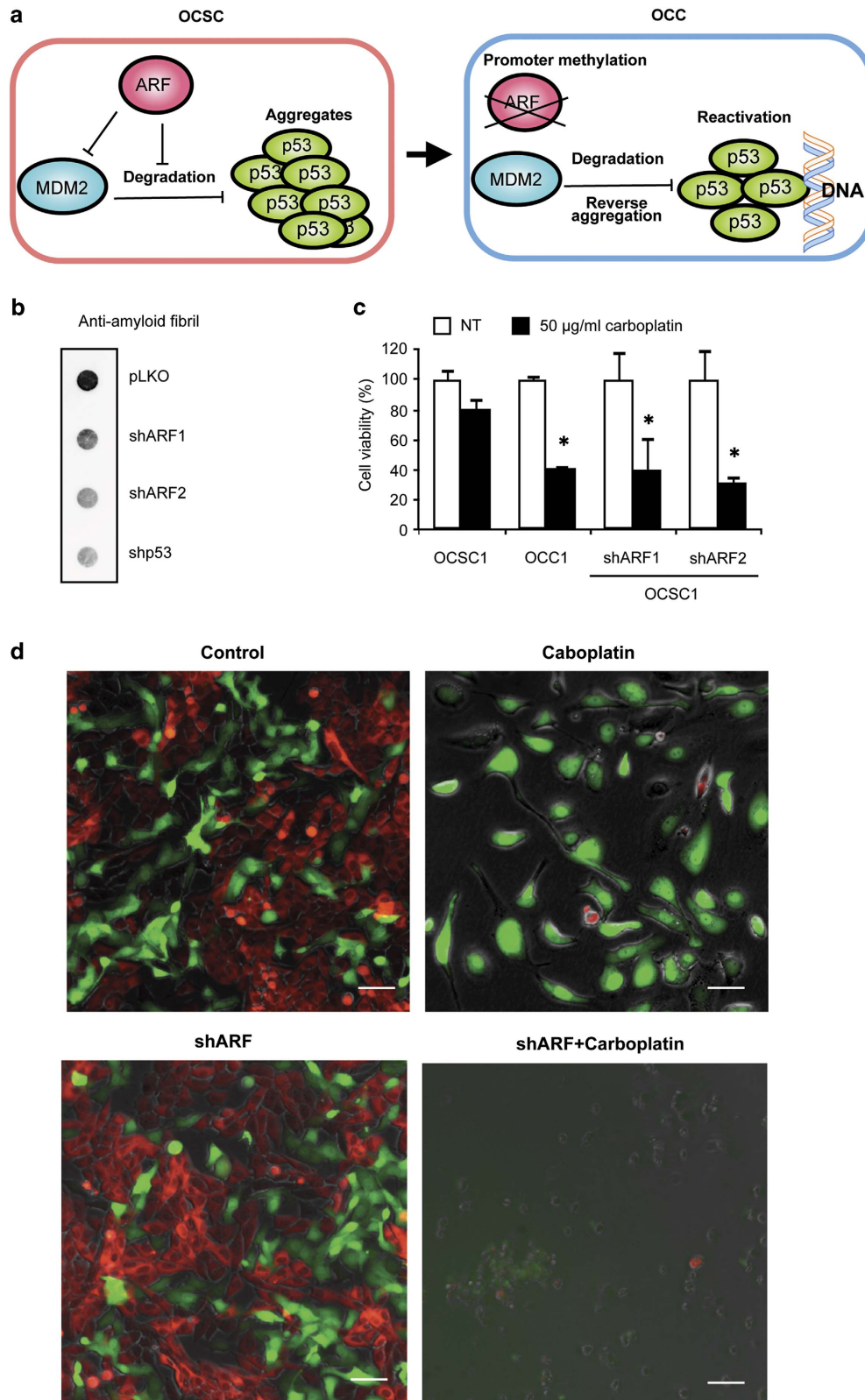


**Figure 4.** ARF silencing reverses p53 aggregation and sensitizes OCSCs *in vitro*. **(a)** Schematic model of p53 regulation in OCSCs (left) and OCCs (right). **(b)** Dot-blot analysis of amyloid fibrils in control pLKO-OCSC1s, shARF1-OCSC1s, shARF2-OCSC1s and shp53-OCSC1s. **(c)** Viability of shARF1-OCSC1s and shARF2-OCSC1s treated by carboplatin. pLKO-OCSC1s and OCC1s are included as chemo-resistant and -sensitive controls, respectively. Data were normalized to respective no treatment controls (NT). \* $P < 0.05$  vs NT. **(d)** Fluorescence images of co-culture model mimicking heterogeneous tumors. GFP-labeled OCSCs or GFP-labeled shARF2-OCSC1s (green) and mCherry-labeled OCCs (red) were mixed and co-cultured. They were treated by carboplatin for 48 h followed by recovery for 48 h. Scale bars are 36  $\mu$ m.

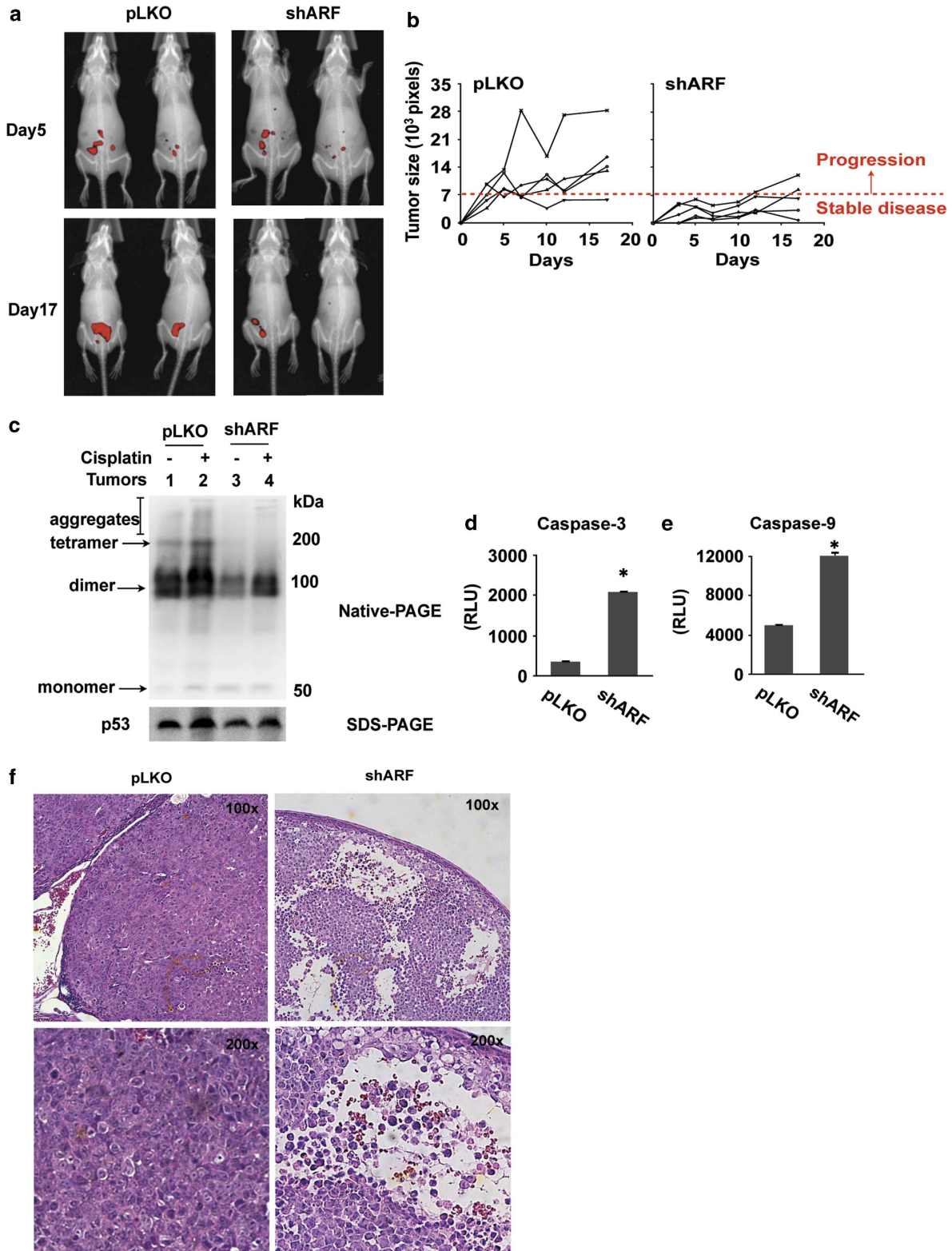


**Figure 5.** ARF silencing reverses p53 aggregation and sensitizes OCSCs *in vivo*. **(a)** Representative images of cisplatin-treated mice with tumors (red) formed by mCherry-labeled pLKO-OCSC1s or shARF2-OCSC1s. **(b)** Growth curves of cisplatin-treated tumors formed by control pLKO-OCSC1s (left,  $n = 5$ ) and shARF2-OCSC1s (right,  $n = 5$ ). Tumor size was quantified by the total number of pixels in the fluorescent areas of the image. Each curve represents the tumor growth in one mouse. The red dotted line indicates the cutoff baseline between stable disease and progression. **(c)** P53 western blot of non-denaturing gel analysis of tumors formed by pLKO-OCSC1s (lanes 1 and 2) or shARF2-OCSC1s (lanes 3 and 4) nontreated (-) or treated (+) with cisplatin. The aggregated p53 protein was detected as the p53 bands at high molecular weight (high MW p53). **(d, e)** Caspase-3 and caspase-9 activity in cisplatin-treated tumors ( $n = 3$ ;  $*P < 0.005$ ) formed by pLKO-OCSC1s (pLKO) and shARF-OCSC1s (shARF). **(f)** Hematoxylin and eosin (H&E) staining of tumors from mice treated by cisplatin.

wide spectrum of p53 mutations will be further investigated in our future study.

## MATERIALS AND METHODS

### Human tissue specimens and cells

CD44+ ovarian cancer cells were isolated from stage III/IV serous ovarian carcinoma samples as previously described.<sup>11</sup> Sample collection was

carried out with patient consent and approved by the Human Investigations Committee of Yale University School of Medicine. Ovarian cancer cells were propagated as previously described.<sup>11,12</sup>

### Flow cytometry

Flow cytometry analysis was performed as previously described.<sup>29</sup> Antibodies include anti-CD44-FITC (no. 11-0441-81, eBioscience, San Diego, CA, USA) and control Isotype-FITC (Sungene Biotech, Tianjin, China).

### Transient transfection

Cells were transfected with pcDNA3-MDM2 (Addgene, Cambridge, MA, USA, plasmid no. 16233) or pcDNA3 (Invitrogen, Carlsbad, CA, USA) plasmid using FuGENE 6 Transfection Reagent (Roche Diagnostics, Indianapolis, IN, USA) according to the manufacturer's instructions. Transfected cells were grown up to 48 h before proteins were extracted.

### Lentiviral infections

Two lentiviral shRNAs targeting ARF and pLKO.1-puro empty vector (Open Biosystems, Huntsville, AL, USA) were produced as previously described.<sup>50</sup> The shRNA and control lentivirus were introduced to OCSC cells by adding to cell growth medium. Then, stable knockdown or control cells were selected by medium containing 1 µg/ml puromycin (Sigma-Aldrich, Milwaukee, WI, USA).

### Cell growth and viability assays

Cell growth and morphology were assessed using Incucyte (Essen Instruments, Ann Arbor, MN, USA). Cell viability was determined with CellTiter 96 AQueous One Solution Cell Proliferation Assay (Promega, Madison, WI, USA) according to the manufacturer's instructions. The viability of treated cells was normalized to the untreated control.

### Immunoblotting

Western blot was performed as previously described.<sup>51</sup> Antibodies were diluted as following: anti-p14ARF (1:1000, no. 2407; Cell Signaling Technology, Beverly, MA, USA), anti-p53 (1:2000, no. OP43; Millipore, Billerica, MA, USA), anti-MDM2 (1:1000, no. OP115; Millipore) and GAPDH (1:10 000, Sigma-Aldrich).

Dot-blot analysis was performed as previously described.<sup>52</sup> Anti-amyloid fibril OC (1:1000, no. AB2286; Millipore) was used to detect protein aggregates. The intensity of the dots was analyzed

| Cellular functions            | P53 aggregates binding proteins   |
|-------------------------------|---|
| Cytoskeleton-related proteins | PLEC1, MYH9, MYH10, EPPK1, ACTN1, AXTN4, DYNC1H1, FLNA, FLNC, SPTAN1, SPTBN1, EVPL, VIM |
| Molecular chaperones          | HSP90AA1, HSP90AB1, HSP90AA2, HSP90B1   |
| Scaffold proteins             | IQGAP1  |
| Exocytosis                    | ANXA1   |
| Cytokinesis                   | CIT   |
| Protein degradation           | PSMD2   |
| Translation                   | EIF2A, EIF2S1, EIF3A, EIF3B, EIF3J, EEF1D, RPS3   |
| tRNA synthetases              | QARS  |
| Mitochondria                  | IMMT, NDUFA9  |
| Metabolism                    | FASN, CAD, MOGS, MTHFD1, LDHB   |
| Nuclear structure             | AHNAK   |
| Ribosome biogenesis           | RPLP0, RPL5, RPL6   |
| RNA processing                | DDX21, SFPQ, CDC5L, WBP11, ILF3   |
| Transcription                 | NCL, SFPQ, SND1, CDC5L  |
| DNA replication               | MCM3, MCM4, MCM5, TOP1  |
| Unspecified                   | EPPK1, TTC13, NPEPPS  |

Abbreviations: OCSC, ovarian cancer stem cell; tRNA, transfer RNA. OCSC1s and OCC1s were treated with carboplatin. Their p53 protein complex was immunoprecipitated and analyzed by two-dimensional gel electrophoresis. The proteins that showed significantly greater (> 5-fold) enrichment in p53 complex of OCSC1s were identified by mass spectrometry. They are listed and classified according to their cellular functions.

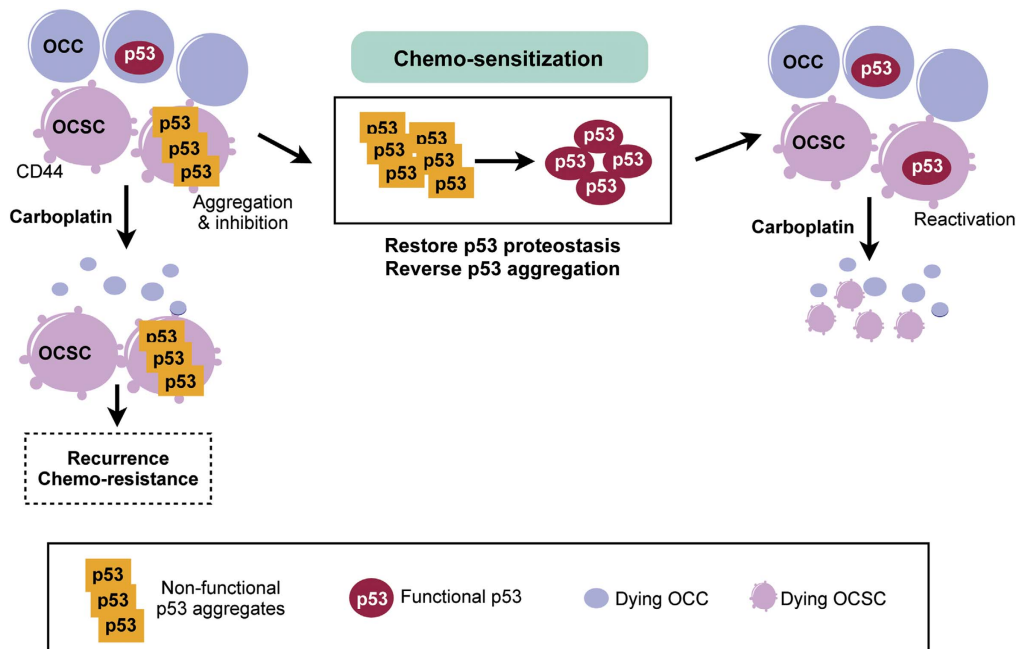


**Figure 6.** Schematic model of chemosensitization targeting p53 protein aggregation.

using Image Analysis Software (Kodak Scientific Imaging Systems, Rochester, NY, USA).

#### Quantitative real-time PCR

Total RNA was extracted from cells or tumor tissues using an RNeasy Mini Kit (Qiagen, Austin, TX, USA) according to the manufacturer's instructions. cDNA was synthesized with Verso cDNA Kit (Thermo Scientific, Waltham, MA, USA) according to the manufacturer's instructions. Quantification of mRNA was performed using KAPA SYBR FAST qPCR Kit (KAPA Biosystems, Woburn, MA, USA) and CFX96TM PCR detection system (Bio-Rad, Hercules, CA, USA). GAPDH was used as reference gene. Relative expression was calculated using the comparative  $\Delta\Delta CT$  method. Primer sequences are listed in Supplementary Table 4.

#### P53 cDNA and DNA sequencing

The p53 cDNA was used as a template to amplified full-length p53 by PCR reaction as previously described.<sup>53</sup> Genomic DNA was extracted with a DNeasy Blood and Tissue Kit (Qiagen). Exons 5–8 of TP53 were amplified by PCR. The purified PCR products were sequenced using the same primers as PCR listed in Supplementary Table 4.

#### Chromatin immunoprecipitation

Chromatin immunoprecipitation was performed as previously described.<sup>54</sup> Anti-p53 antibody (no. OP43, EMD Millipore, Temecula, CA, USA) was added to the test groups. Mouse IgG (sc-2025, Santa Cruz Biotechnology, Dallas, TX, USA) was added to the immunoprecipitation (IP) control groups.

Quantitative PCR primer sequences are listed in Supplementary Table 4. GAPDH is used as the negative control. The PCR data of IP test and IgG control groups were both normalized to input control group. After normalization, the signals of IP p53 samples are divided by the signals of IgG control sample to get the fold of increase in IP p53 signal relative to the background signal. At last, the data of OCSC1 and OCC1 were divided by the nontreated OCSC1. The data of OCSC2 and OCC2 were divided by the nontreated OCC2. The final step is comparing p53 DNA binding between OCSCs and their daughter cell lines OCCs upon carboplatin treatment.

#### Methylation-specific PCR

DNA methylation patterns in the CpG islands of the p14ARF gene were determined by methylation-specific PCR as previously described.<sup>55</sup> Primer sequences are listed in Supplementary Table 4. Normal human ovarian surface epithelial cells were used as negative control (unmethylated alleles). The DNA of ovarian surface epithelial cells that was treated *in vitro* with Sssl CpG methyltransferase at 37 °C for 1 h was used as a positive control (methylated alleles).

#### Immunocytofluorescence costaining

Adherent cells on 8-chamber glass LabTek culture slides (BD Falcon, Bedford, MA, USA) were fixed with ice-cold 3.7% paraformaldehyde for 5 min and permeabilized using 0.2% Triton X-100. The slides were then blocked in 10% normal goat serum and incubated at room temperature with anti-p53 antibody (1:500, no. OP43, EMD Millipore) for 1 h and then AlexaFluor-546-labeled goat anti-mouse IgG antibody (Invitrogen) for 1 h. For amyloid fibril staining, slides were incubated with anti-amyloid fibril antibody (1:1000, no. AB2286 Millipore) at 4 °C overnight, then with AlexaFluor-488-labeled donkey anti-rabbit IgG antibody (1:1000, Life Technologies, Carlsbad, CA, USA) at room temperature for 1 h. For thioflavin T staining, after p53 staining, slides were incubated in thioflavin T (5 mM in phosphate-buffered saline) for 10 min at room temperature. The slides were washed with 70% ethanol for 5 min twice and then rinsed with distilled water 3 times.

Nuclei were stained using 4',6-diamidino-2-phenylindole. Between each blocking or staining step, the slides were washed by phosphate-buffered saline 3 times. The slides were cover-slipped using Fluorescence Mounting Medium (Dako, Glostrup, Denmark) and captured with Zeiss Axio Observer inverted fluorescence microscope (Carl Zeiss, Oberkochen, Germany). Acquisition settings were kept constant.

#### Identification of aggregated p53-binding proteins

Immunoprecipitation of p53 was performed on carboplatin (100  $\mu\text{g}/\text{ml}$ , 24 h)-treated OCSC1s and OCC1s as previously described<sup>56</sup> with anti-p53 (1  $\mu\text{g}/\text{ml}$ , no. OP43, EMD Millipore) antibody. The precipitated p53 complex was proceeded to two-dimensional gel. The two-dimensional gel analysis was performed as previously described.<sup>57</sup> The gel spots with fivefold greater intensity in the gel of OCSC1s than OCC1s were picked for identification by liquid chromatography tandem mass spectrometry analysis. The liquid chromatography tandem mass spectrometry was performed as previously described.<sup>58</sup> Proteins that had at least three fragments identified by liquid chromatography tandem mass spectrometry were selected as positive candidates.

#### Xenograft experiments

Yale University Institutional Animal Care and Use Committee approved this protocol. Six-week-old female athymic nude mice (Harlan, South Easton, MA, USA) were maintained under pathogen-free conditions, and food and water were supplied *ad libitum*. In the subcutaneous and intraperitoneal xenograft models,  $3 \times 10^6$  and  $7 \times 10^6$  cells were injected, respectively. At 7 days post injection, mice were treated with cisplatin at 5  $\mu\text{g}/\text{kg}$  body weight once per week. Tumors were monitored by Carestream *In-Vivo* Imaging System. Images were quantified by Carestream software (Carestream Health, Woodbridge, CT, USA). Tumor size was measured by creating an automatic region of interest and measuring that area's pixel number.

#### Statistical analyses

Numerical values are reported as the mean  $\pm$  s.d. For comparisons between two groups, *P*-values were calculated using unpaired two-tailed Student's *t*-tests. For the correlation analysis, *P*-values were calculated using Fisher's exact test. *P*-values of  $\leq 0.05$  were considered statistically significant.

#### CONFLICT OF INTEREST

The authors declare no conflict of interest.

#### ACKNOWLEDGEMENTS

This study was supported by NIH Grants RO1CA118678 and RO1CA127913, Sands Family Foundation and Discovery to Cure Program. We thank Drs Alice Soragni and David Eisenberg of UCLA for their suggestion that aggregated p53 could act as a potential therapeutic target.

#### REFERENCES

- 1 Clarke-Pearson DL. Clinical practice. Screening for ovarian cancer. *N Engl J Med* 2009; **361**: 170–177.
- 2 Cancer Genome Atlas Research Network. Integrated genomic analyses of ovarian carcinoma. *Nature* 2011; **474**: 609–615.
- 3 UMD TP53 mutation database. <http://p53.fr/>.
- 4 IARC TP53 Database. <http://www.iarc.fr/p53/Index.html>.
- 5 Freed-Pastor WA, Prives C. Mutant p53: one name, many proteins. *Genes Dev* 2012; **26**: 1268–1286.
- 6 Moll UM, Riou G, Levine AJ. Two distinct mechanisms alter p53 in breast cancer: mutation and nuclear exclusion. *Proc Natl Acad Sci USA* 1992; **89**: 7262–7266.
- 7 Tominaga O, Hamelin R, Trouvat V, Salmon RJ, Lesec G, Thomas G *et al*. Frequently elevated content of immunochemically defined wild-type p53 protein in colorectal adenomas. *Oncogene* 1993; **8**: 2653–2658.
- 8 Houben R, Hesbacher S, Schmid CP, Kauczok CS, Flohr U, Haferkamp S *et al*. High-level expression of wild-type p53 in melanoma cells is frequently associated with inactivity in p53 reporter gene assays. *PLoS ONE* 2011; **6**: e22096.
- 9 Wong KK, Izaguirre DI, Kwan SY, King ER, Deavers MT, Sood AK *et al*. Poor survival with wild-type TP53 ovarian cancer? *Gynecol Oncol* 2013; **130**: 565–569.
- 10 Silva JL, Rangel LP, Costa DC, Cordeiro Y, De Moura Gallo CV. Expanding the prion concept to cancer biology: dominant-negative effect of aggregates of mutant p53 tumour suppressor. *Biosci Rep* 2013; **33**: 593–603.
- 11 Xu J, Reumers J, Couceiro JR, De Smet F, Gallardo R, Rudyak S *et al*. Gain of function of mutant p53 by coaggregation with multiple tumor suppressors. *Nat Chem Biol* 2011; **7**: 285–295.

- 12 Ano Bom AP, Rangel LP, Costa DC, de Oliveira GA, Sanches D, Braga CA *et al*. Mutant p53 aggregates into prion-like amyloid oligomers and fibrils: implications for cancer. *J Biol Chem* 2012; **287**: 28152–28162.
- 13 Levy CB, Stumbo AC, Ano Bom AP, Portari EA, Cordeiro Y, Silva JL *et al*. Co-localization of mutant p53 and amyloid-like protein aggregates in breast tumors. *Int J Biochem Cell Biol* 2011; **43**: 60–64.
- 14 Stefani M, Dobson CM. Protein aggregation and aggregate toxicity: new insights into protein folding, misfolding diseases and biological evolution. *J Mol Med (Berl)* 2003; **81**: 678–699.
- 15 Higashimoto Y, Asanomi Y, Takakusagi S, Lewis MS, Uosaki K, Durell SR *et al*. Unfolding, aggregation, and amyloid formation by the tetramerization domain from mutant p53 associated with lung cancer. *Biochemistry* 2006; **45**: 1608–1619.
- 16 Ishimaru D, Andrade LR, Teixeira LS, Quesado PA, Maiolino LM, Lopez PM *et al*. Fibrillar aggregates of the tumor suppressor p53 core domain. *Biochemistry* 2003; **42**: 9022–9027.
- 17 Rigacci S, Bucciantini M, Relini A, Pesce A, Gliozzi A, Berti A *et al*. The (1–63) region of the p53 transactivation domain aggregates in vitro into cytotoxic amyloid assemblies. *Biophys J* 2008; **94**: 3635–3646.
- 18 Butler JS, Loh SN. Structure, function, and aggregation of the zinc-free form of the p53 DNA binding domain. *Biochemistry* 2003; **42**: 2396–2403.
- 19 Ishimaru D, Lima LM, Maia LF, Lopez PM, Ano Bom AP, Valente AP *et al*. Reversible aggregation plays a crucial role on the folding landscape of p53 core domain. *Biophys J* 2004; **87**: 2691–2700.
- 20 Olzsch A, Schermann SM, Woerner AC, Pinkert S, Hecht MH, Tartaglia GG *et al*. Amyloid-like aggregates sequester numerous metastable proteins with essential cellular functions. *Cell* 2011; **144**: 67–78.
- 21 Forget KJ, Tremblay G, Roucou X. p53 aggregates penetrate cells and induce the co-aggregation of intracellular p53. *PLoS ONE* 2013; **8**: e69242.
- 22 Lasagna-Reeves CA, Clos AL, Castillo-Carranza D, Sengupta U, Guerrero-Munoz M, Kelly B *et al*. Dual role of p53 amyloid formation in cancer; loss of function and gain of toxicity. *Biochem Biophys Res Commun* 2013; **430**: 963–968.
- 23 Al-Hajj M, Wicha MS, Benito-Hernandez A, Morrison SJ, Clarke MF. Prospective identification of tumorigenic breast cancer cells. *Proc Natl Acad Sci USA* 2003; **100**: 3983–3988.
- 24 Richardson GD, Robson CN, Lang SH, Neal DE, Maitland NJ, Collins AT. CD133, a novel marker for human prostatic epithelial stem cells. *J Cell Sci* 2004; **117**(Pt 16): 3539–3545.
- 25 Shih Ie M, Davidson B. Pathogenesis of ovarian cancer: clues from selected overexpressed genes. *Future Oncol* 2009; **5**: 1641–1657.
- 26 Peng S, Maihle NJ, Huang Y. Pluripotency factors Lin28 and Oct4 identify a sub-population of stem cell-like cells in ovarian cancer. *Oncogene* 2010; **29**: 2153–2159.
- 27 Rizzo S, Hersey JM, Mellor P, Dai W, Santos-Silva A, Liber D *et al*. Ovarian cancer stem cell-like side populations are enriched following chemotherapy and overexpress EZH2. *Mol Cancer Ther* 2011; **10**: 325–335.
- 28 Steg AD, Bevis KS, Katre AA, Ziebarth A, Dobbin ZC, Alvarez RD *et al*. Stem cell pathways contribute to clinical chemoresistance in ovarian cancer. *Clin Cancer Res* 2012; **18**: 869–881.
- 29 Alvero AB, Chen R, Fu HH, Montagna M, Schwartz PE, Rutherford T *et al*. Molecular phenotyping of human ovarian cancer stem cells unravels the mechanisms for repair and chemoresistance. *Cell Cycle* 2009; **8**: 158–166.
- 30 Alvero AB, Fu HH, Holmberg J, Visintin I, Mor L, Marquina CC *et al*. Stem-like ovarian cancer cells can serve as tumor vascular progenitors. *Stem Cells* 2009; **27**: 2405–2413.
- 31 Chen R, Alvero AB, Silasi DA, Kelly MG, Fest S, Visintin I *et al*. Regulation of IKKbeta by miR-199a affects NF-kappaB activity in ovarian cancer cells. *Oncogene* 2008; **27**: 4712–4723.
- 32 Craveiro V, Yang-Hartwich Y, Holmberg JC, Sumi NJ, Pizzonia J, Griffin B *et al*. Phenotypic modifications in ovarian cancer stem cells following Paclitaxel treatment. *Cancer Med* 2013; **2**: 751–762.
- 33 Aguzzi A, O'Connor T. Protein aggregation diseases: pathogenicity and therapeutic perspectives. *Nat Rev Drug Discov* 2010; **9**: 237–248.
- 34 Zhang Y, Xiong Y, Yarbrough WG. ARF promotes MDM2 degradation and stabilizes p53: ARF-INK4a locus deletion impairs both the Rb and p53 tumor suppression pathways. *Cell* 1998; **92**: 725–734.
- 35 Pomerantz J, Schreiber-Agus N, Liegeois NJ, Silverman A, Alland L, Chin L *et al*. The Ink4a tumor suppressor gene product, p19Arf, interacts with MDM2 and neutralizes MDM2's inhibition of p53. *Cell* 1998; **92**: 713–723.
- 36 Tao W, Levine AJ. P19(ARF) stabilizes p53 by blocking nucleo-cytoplasmic shuttling of Mdm2. *Proc Natl Acad Sci USA* 1999; **96**: 6937–6941.
- 37 Weber JD, Taylor LJ, Roussel MF, Sherr CJ, Bar-Sagi D. Nucleolar Arf sequesters Mdm2 and activates p53. *Nat Cell Biol* 1999; **1**: 20–26.
- 38 Iwakuma T, Lozano G. MDM2: an introduction. *Mol Cancer Res* 2003; **1**: 993–1000.
- 39 Rayburn E, Zhang R, He J, Wang H. MDM2 and human malignancies: expression, clinical pathology, prognostic markers, and implications for chemotherapy. *Curr Cancer Drug Targets* 2005; **5**: 27–41.
- 40 Biancalana M, Koide S. Molecular mechanism of Thioflavin-T binding to amyloid fibrils. *Biochim Biophys Acta* 2010; **1804**: 1405–1412.
- 41 Kaye R, Head E, Sarsoza F, Saing T, Cotman CW, Necula M *et al*. Fibril specific, conformation dependent antibodies recognize a generic epitope common to amyloid fibrils and fibrillar oligomers that is absent in prefibrillar oligomers. *Mol Neurodegener* 2007; **2**: 18.
- 42 Zheng S, Chen P, McMillan A, Lafuente A, Lafuente MJ, Ballesta A *et al*. Correlations of partial and extensive methylation at the p14(ARF) locus with reduced mRNA expression in colorectal cancer cell lines and clinicopathological features in primary tumors. *Carcinogenesis* 2000; **21**: 2057–2064.
- 43 Ciechanover A. The ubiquitin proteolytic system: from a vague idea, through basic mechanisms, and onto human diseases and drug targeting. *Neurology* 2006; **66**(2 Suppl 1): S7–19.
- 44 Wong E, Cuervo AM. Autophagy gone awry in neurodegenerative diseases. *Nat Neurosci* 2010; **13**: 805–811.
- 45 Kraiss S, Spiess S, Reihnsaus E, Montenarh M. Correlation of metabolic stability and altered quaternary structure of oncoprotein p53 with cell transformation. *Exp Cell Res* 1991; **192**: 157–164.
- 46 Wilcken R, Wang G, Boeckler FM, Fersht AR. Kinetic mechanism of p53 oncogenic mutant aggregation and its inhibition. *Proc Natl Acad Sci USA* 2012; **109**: 13584–13589.
- 47 Silva JL, Gallo CV, Costa DC, Rangel LP. Prion-like aggregation of mutant p53 in cancer. *Trends Biochem Sci* 2014; **39**: 260–267.
- 48 Albor A, Kaku S, Kulesz-Martin M. Wild-type and mutant forms of p53 activate human topoisomerase I: a possible mechanism for gain of function in mutants. *Cancer Res* 1998; **58**: 2091–2094.
- 49 Peng Y, Chen L, Li C, Lu W, Chen J. Inhibition of MDM2 by hsp90 contributes to mutant p53 stabilization. *J Biol Chem* 2001; **276**: 40583–40590.
- 50 Tiscornia G, Singer O, Verma IM. Production and purification of lentiviral vectors. *Nat Protoc* 2006; **1**: 241–245.
- 51 Kamsteeg M, Rutherford T, Sapi E, Hanczaruk B, Shahabi S, Flick M *et al*. Phenoxodiol—an isoflavone analog—induces apoptosis in chemoresistant ovarian cancer cells. *Oncogene* 2003; **22**: 2611–2620.
- 52 Kaye R, Glabe CG. Conformation-dependent anti-amyloid oligomer antibodies. *Methods Enzymol* 2006; **413**: 326–344.
- 53 Szybka M, Zakrzewska M, Rieseke P, Pasz-Walczak G, Kulczycka-Wojdala D, Zawlik I *et al*. cDNA sequencing improves the detection of P53 missense mutations in colorectal cancer. *BMC Cancer* 2009; **9**: 278.
- 54 Wells J, Farnham PJ. Characterizing transcription factor binding sites using formaldehyde crosslinking and immunoprecipitation. *Methods* 2002; **26**: 48–56.
- 55 Klump B, Hsieh CJ, Dette S, Holzmann K, Kiebetalch R, Jung M *et al*. Promoter methylation of INK4a/ARF as detected in bile-significance for the differential diagnosis in biliary disease. *Clin Cancer Res* 2003; **9**: 1773–1778.
- 56 Erica Golemis PDA (ed) *Protein-Protein Interactions: A Molecular Cloning Manual*. Cold Spring Harbor Laboratory Press: Cold Spring Harbor, NY, 2002.
- 57 Wu TL. Two-dimensional difference gel electrophoresis. *Methods Mol Biol* 2006; **328**: 71–95.
- 58 Dieguez-Acuna F, Kodama S, Okubo Y, Paz AC, Gygi SP, Faustman DL. Proteomics identifies multipotent and low oncogenic risk stem cells of the spleen. *Int J Biochem Cell Biol* 2010; **42**: 1651–1660.

Supplementary Information accompanies this paper on the Oncogene website (<http://www.nature.com/onc>)